

# Numerical simulation on cavitation pressure fluctuation in centrifugal pump at low flow rate

G Q Q G MENG<sup>1\*</sup>, X F YAN<sup>1</sup> and X WANG<sup>1,2</sup>

<sup>1</sup> Inner Mongolia Vocational College of Chemical Engineering, Hohhot 010070, Inner Mongolia, China

<sup>2</sup> Inner Mongolia University of Technology, Hohhot 010051, Inner Mongolia, China

E-mail: erenmangha2012@163.com

**Abstract.** The RNG  $\kappa$ - $\varepsilon$  turbulence model and the modified mass transport cavitation model are applied to simulate the unsteady cavitation flows in a centrifugal pump at low flow rate. Unsteady cavitation flows analyses in centrifugal pump are focused mainly in the volute. The accuracy and reliability of the numerical model and method are demonstrated by the good agreement between with experimental and numerical values of the pump performance. 13 monitor points are positioned in the volute. The time domain and frequency domain of pressure fluctuations on monitor points are analyzed and discussed. Under different conditions, the pressure fluctuation at each monitoring positions has obvious periodic property. The intensity of pressure fluctuation gets stronger with the development of pump cavitation. The dominant frequency of pressure fluctuations in volute is the blade pass frequency ( $f_{BPF}$ ) and its harmonic frequency. Under cavitation condition, the pressure fluctuations is the most intense in the volute diffusion tube, and the maximum amplitudes is about 2~3 times of non-cavitation. It is indicate that cavitation has a great influence on the outlet flow field of centrifugal pump.

## 1. Introduction

Cavitation is a common phenomenon in the operation of the centrifugal pump. The cavitation bubbles collapse induces pressure fluctuation in the pump. Thus, a technique allowing for the prediction and control of pressure fluctuation in the pump induced by cavitation is needed at the design stage. The half of blade passing frequency (BPF) is more sensitive on the cavitation development in a centrifugal pump [1,2]. For the cavitation condition, the large scale low-frequency oscillations appears in centrifugal pump [3]. The size of shock wave that induced by the collapse of bubbles influences the cavity shedding frequency [4].

The unsteady characteristics of cavitation flows in centrifugal pump are still difficult to capture accurately [5], especially under off-design conditions [6]. Hence modified calculation model is widely used [7,8]. In this paper, the unsteady cavitation flows in a centrifugal pump at low flow rate  $Q=19.80\text{m}^3/\text{h}$  is calculated by using the RNG  $k$ - $\varepsilon$  turbulence model and modified mass transport cavitation model. Also, the experiments are carried out to validate the numerical simulations. From these results, the characteristics of pressure fluctuations in the volute is analyzed.

## 2. Case description and numerical algorithm

### 2.1. Parameter of centrifugal pump and computational domain



The main parameters of the centrifugal pump are as follows: the design flow rate  $Q_d=25\text{m}^3/\text{h}$ , the rotational speed  $n=1450\text{r}/\text{min}$ , the pump head  $H=7\text{m}$ , the number of blades  $Z=7$ , the wrap angle of pump is  $98^\circ$ , the inlet diameter is  $50\text{mm}$  and outlet diameter is  $160\text{mm}$ . Figure 1 shows the computational domain and mesh of the centrifugal pump. The computational domain consists of three modules, as shown in figure 1(a). All the meshes are structural mesh in the computational domain, as shown in figure 1(b) and 1(c).

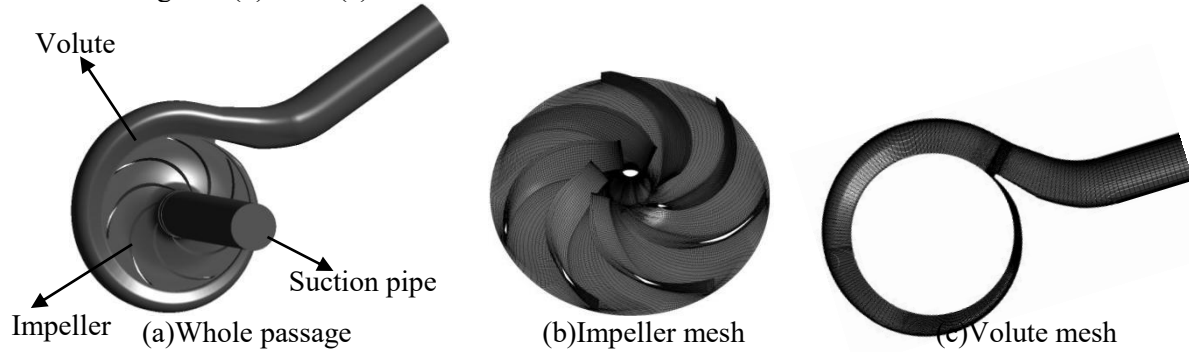


**Figure 1.** Computation domain and mesh of centrifugal pump.

## 2.2. Mesh density and time step independence

Five different mesh densities from 1,562,765 to 2,629,005 are adopted to test the mesh independence, as shown in table 1. The results indicate that the pump head  $H$  differences is very tiny for the five mesh densities, hence the 1,562,765 elements is employed for the following calculation.

**Table 1.** Mesh independence.

Item	1	2	3	4	5
Suction pipe zone	575740	575740	575740	575740	575740
Volute zone	661105	661105	661105	661105	661105
Impeller zone	325920	600768	892584	1139040	1392160
Whole passage	1562765	1837613	2129429	2375885	2629005
$H/H_1$	1	1.005674	1.002829	1.004249	1.008535

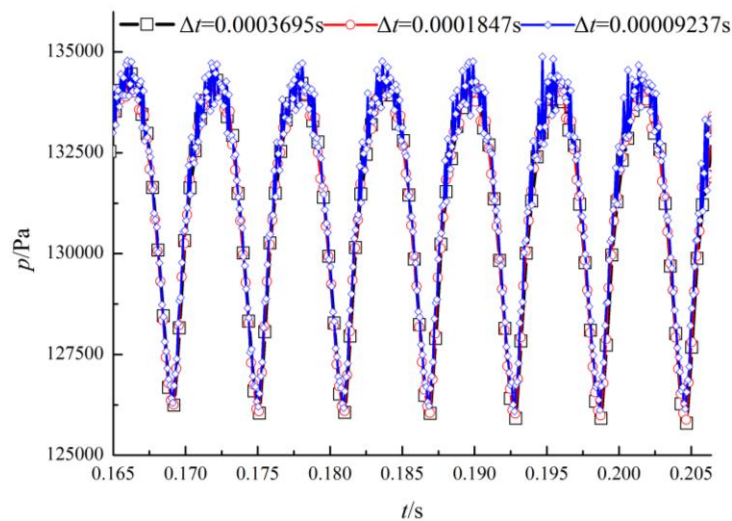


**Figure 2.** Monitored pressure at different time steps.

Three sets of time steps  $\Delta t=3.695 \times 10^{-4}$ s,  $1.847 \times 10^{-4}$ s and  $0.924 \times 10^{-4}$ s are adopted to test the time step independence. The monitored pressure in the pump outlet at the 3 different time steps, shown in figure 2. The results showed that the 3 sets of time step differences is very tiny, so choose time step  $\Delta t=1.847 \times 10^{-4}$ s.

### 2.3. Numerical model and method

The fluid is considered as a homogeneous and compressible mixed medium. The continuity and momentum equations in the Cartesian coordinates are as follows:

$$\frac{\partial \rho_m}{\partial t} + \nabla \cdot (\rho_m U) = 0 \quad (1)$$

$$\frac{\partial}{\partial t}(\rho_m U) + \nabla \cdot (\rho_m U \cdot U) = -\nabla p + \nabla \cdot [(\mu_m + \mu_t) \nabla U] + \frac{1}{3} \nabla [(\mu_m + \mu_t) \nabla \cdot U] \quad (2)$$

Where  $\rho$  and  $\mu$  are the density and dynamic viscosity, calculated by weighted average of each phase volume fraction  $\alpha$ ,  $\rho_m = \rho_l \alpha_l + \rho_v \alpha_v$ ,  $\mu_m = \mu_l \alpha_l + \mu_v \alpha_v$ ; subscripts  $l$ ,  $v$  and  $m$  denote the liquid phase, the vapor phase and the mixture, respectively;  $U$  is the velocity vector,  $p$  is the pressure, and  $\mu_t$  is the turbulent viscosity.

The widely applied RNG  $k$ - $\epsilon$  turbulence model is used.

The mass transport cavitation model is considered in this paper, the liquid-vapor mass transfers due to cavitation are solved by transport equation.

$$\frac{\partial (\rho_v \alpha_v)}{\partial t} + \nabla \cdot (\rho_v \alpha_v u) = \dot{m}_{vap} - \dot{m}_{con} \quad (3)$$

In which the vaporization rate  $\dot{m}_{vap}$  and condensation rate  $\dot{m}_{con}$  are modeled as

$$\dot{m}_{vap} = C_{vap} \frac{3r_g(1-\alpha_v)\rho_v}{R_b} \sqrt{\frac{2}{3} \frac{\max(p_v - p, 0)}{\rho_l}} \quad (4)$$

$$\dot{m}_{con} = C_{con} \frac{3\alpha_v\rho_v}{R_b} \sqrt{\frac{2}{3} \frac{\max(p - p_v, 0)}{\rho_l}} \quad (5)$$

Where  $\alpha_v$  is the vapor volume fraction,  $u$  is the velocity,  $\rho_v$  is the vapor density,  $r_g$  is the nucleation site volume fraction,  $R_b$  is the nucleation site radius,  $\rho_l$  is the liquid density,  $p_v$  is the water vaporization pressure.  $C_{vap}=50$  and  $C_{con}=0.01$  [9] are the empirical calibration coefficients of vaporization and condensation, respectively. The  $C_{con}$  have great influence on predicting the cavitation performance. In order to improve the numerical simulation accuracy, the empirical calibration coefficient condensation  $C_{con}$  is modified, and  $C_{con}=10^{-4}$  is selected [10,11].

The commercial CFD code CFX14.0 is employed. The boundary conditions are defined as: the total pressure at the pump inlet and mass flow rate at the pump outlet, and the no-slip condition for the boundary layers at the impeller blades and sidewalls, inlet and outlet pipe walls, volute casing. In unsteady calculation, the steady calculated results is the initial value, and the impeller rotation cycle is  $T=0.04138$ s.

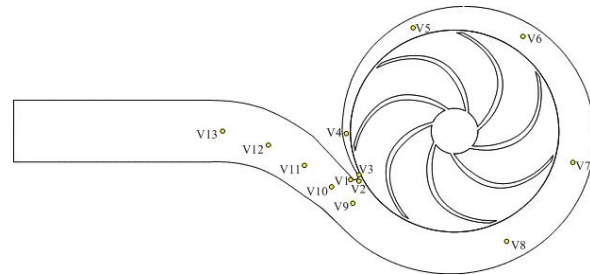
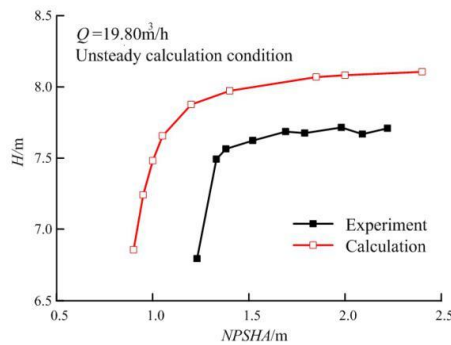
### 2.4. Validation of calculation results

The available net positive suction head ( $NPSHA$ ), defined in equation (6), is the difference between the total energy and vaporization pressure energy for the unit weight of fluid at the pump inlet.

$$NPSHA = \frac{p_1}{\rho_l g} + \frac{u_1^2}{2g} - \frac{p_v}{\rho_l g} \quad (6)$$

Where  $p_1$  is the pump inlet pressure and  $u_1$  is the pump inlet speed.

Figure 3 shows the calculated variation of pump head with the available net positive suction head is compared with the experimental results. The  $NPSHA$  by calculation are higher than those by experiment, and the calculated variation of pump head is in good agreement with the experimental data as shown in figure 3.

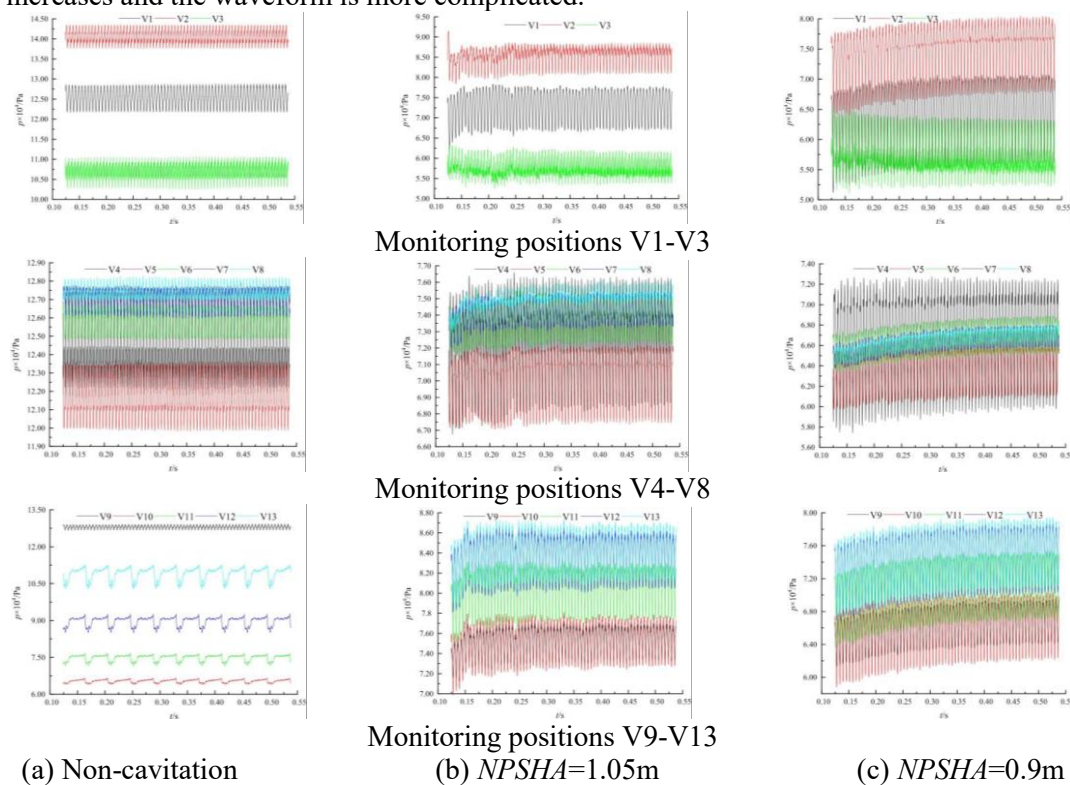
**Figure 3.** Relationship between pump head and *NPSHA*.**Figure 4.** Monitoring positions in volute.

### 3. Results and discussion

#### 3.1. Pressure fluctuation characteristics in volute

In the calculation of unsteady cavitation flows, *NPSHA*=1.05m and 0.9m are selected to analysis. The total time is using 10 impeller rotation cycles to calculate, and the characteristics of pressure fluctuation frequency domain is obtained by Fast Fourier Transform. The blade pass Frequency is  $f_{BPF}=nZ/60=169.17\text{Hz}$ . To investigate the unsteady flows in the volute, 13 monitoring points V1-V13 are set along the direction of flow direction, as shown in figure 4.

**3.1.1 Pressure fluctuation time domain.** Under non-cavitation and *NPSHA*=1.05m, 0.9m, the pressure fluctuation time domain of all monitoring points in volute, as shown in figure 5. For non-cavitation and cavitation condition, the 13 monitoring points appears the regular fluctuation in the 10 impeller cycle time. With the decrease of *NPSHA*, the pressure fluctuation amplitudes on each monitoring point increases and the waveform is more complicated.

**Figure 5.** Pressure fluctuation time domain in volute.

**3.1.2 Pressure fluctuation frequency domain.** Under non-cavitation and  $NPSHA=1.05\text{m}$ ,  $0.9\text{m}$ , the pressure fluctuation frequency domain in the volute, as shown in figure 6. With the increase of frequency, the pressure fluctuation amplitudes on each monitoring point decreases gradually.

Under non-cavitation, the pressure fluctuations dominant frequency on V3 and V4 are  $2f_{BPF}$ , on other monitoring points are  $f_{BPF}$ , as shown in figure 6(a). Under  $NPSHA=1.05\text{m}$ , the dominant frequency on V3, V4 and V8 are  $2f_{BPF}$ , on other monitoring points are  $f_{BPF}$ , as shown in figure 6(b). Under  $NPSHA=0.9\text{m}$ , the dominant frequency on V3 and V8 are  $2f_{BPF}$ , on other monitoring points are  $f_{BPF}$ , as shown in figure 6(c).

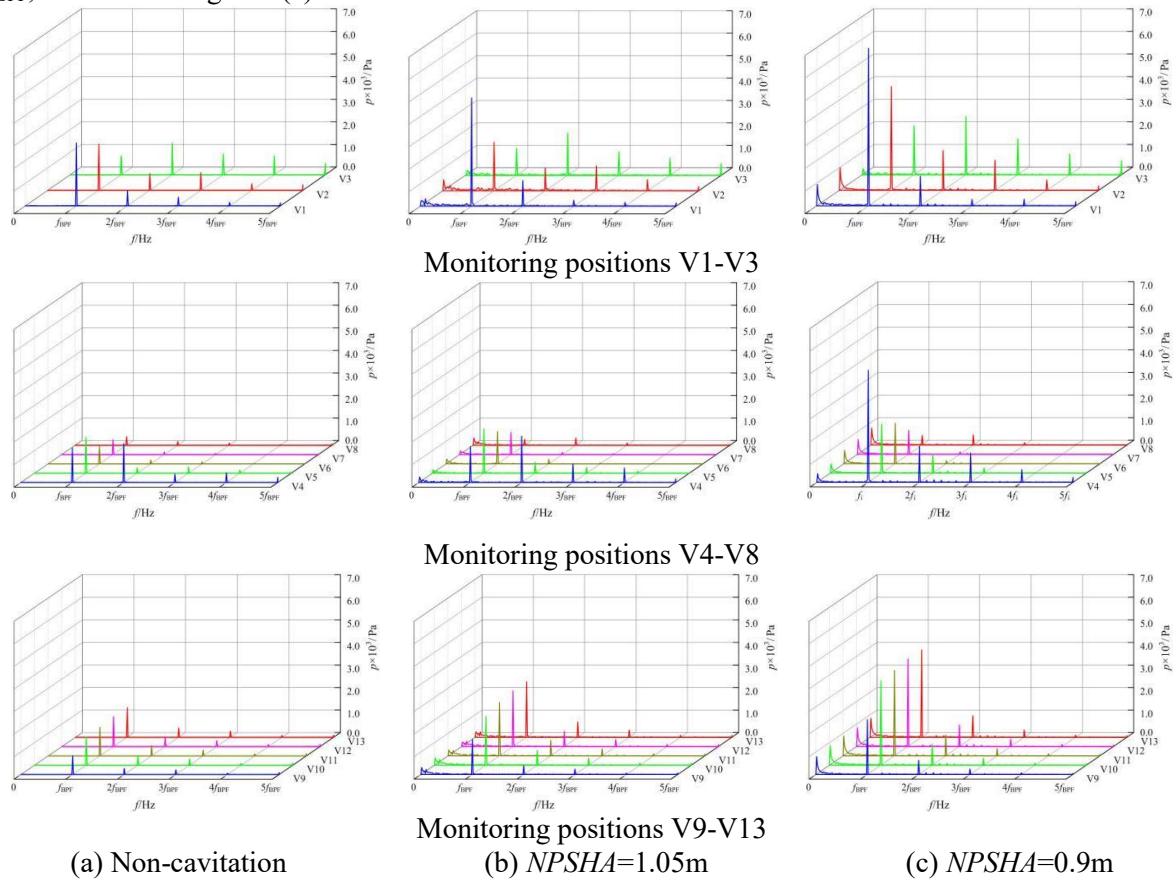


**Figure 6.** Pressure fluctuation frequency domain in volute.

**3.1.3 Maximum amplitude of pressure fluctuation.** Under the non-cavitation and  $NPSHA=1.05\text{m}$ ,  $0.9\text{m}$ , the maximum amplitudes of pressure fluctuation on points V1-V13 in the volute, as shown in table 2. Under non-cavitation and cavitation condition, the maximum amplitude is biggest at point V1. Compared with non-cavitation, it is noteworthy that the maximum amplitude of point V8 decreases at  $NPSHA=1.05\text{m}$ , and on other monitoring points increases significantly. Especially, the monitoring points V1, V6, V9, V10, V11, V12, V13, which value is about 2 times of non-cavitation; under  $NPSHA=0.9\text{m}$ , the maximum amplitudes on all monitoring points are significantly increased, and the monitoring points V4, V8, V9, V10, V11, V12, V13, which value is about 3 times of non-cavitation.



**Table 2.** Maximum amplitude of pressure fluctuation.

Monitoring points	Maximum amplitude of pressure fluctuation/Pa		
	Non-cavitation	$NPSHA=1.05\text{m}$	$NPSHA=0.9\text{m}$
V1	2 778.9	4 831.0	6 958.5
V2	2 037.9	2 167.5	4 583.3
V3	1 395.4	1 890.5	2 575.9
V4	1 718.5	2 047.0	4 943.8
V5	1 589.1	1 964.7	2 156.4
V6	778.7	1 423.4	1 779.6
V7	659.3	983.0	1 052.6
V8	379.2	319.3	441.0
V9	828.6	1 551.7	2 425.3
V10	1 250.6	2 151.8	3 736.4
V11	1 268.2	2 365.4	3 784.7
V12	1 323.7	2 468.8	3 883.3
V13	1 315.6	2 463.2	3 873.5

### 3.2. Flow characteristics in volute

According to the table 2 results, compared with non-cavitation, the maximum amplitude, only on point V8 decreases, and on other monitoring points increases. In order to investigate this phenomenon, the streamline distribution in the volute cross-section V8 under non-cavitation and  $NPSHA=1.05\text{m}$  is listed, as shown in figure 7.

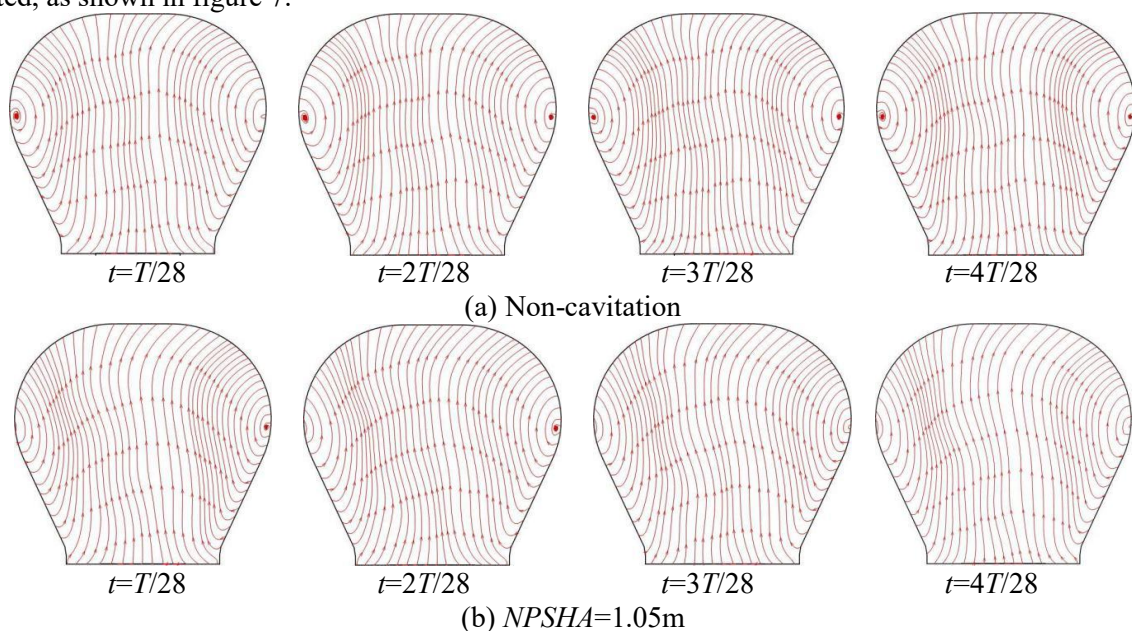
**Figure 7.** Transient flow patterns in cross-section V8.

Figure 7 shows the flow patterns in cross-section middle is relatively smooth, secondary flows at cross-section left and right sides are obvious. Under non-cavitation, at  $t=T/28$ , the vortex appears in volute left side; at  $t=2T/28$ ,  $3T/28$  and  $4T/28$ , the reverse vortex appears in volute left and right sides. Under  $NPSHA=1.05\text{m}$ , at  $t=T/28$  and  $2T/28$ , the vortex in left side disappears; at  $t=3T/28$  and  $4T/28$ , the vortex in right side disappears also. Hence, the vortex strength weakened, led to the amplitude of pressure fluctuation decreases.

#### 4. Conclusion

The unsteady cavitation flows in a centrifugal pump is calculated by using the RNG  $\kappa\text{-}\varepsilon$  turbulence model and modified mass transport cavitation model. The calculated pump performance is in good agreement with the experimental results. The characteristics of pressure fluctuations in volute is analyzed. The main conclusion are as follows:

Under non-cavitation and cavitation condition, the pressure fluctuation in volute have obvious periodic property. The dominant frequency of pressure fluctuations in volute is the blade pass frequency  $f_{BPF}$  and  $2f_{BPF}$ . With the development of pump cavitation, the amplitudes of pressure fluctuations in volute increases basically.

Compared with the non-cavitation, the maximum amplitudes of pressure fluctuation in the volute diffusion tube are increased significantly, and under  $NPSHA=1.05\text{m}$ , amplitudes value about 2 times of non-cavitation, under  $NPSHA=0.9\text{m}$ , about 3 times of non-cavitation.

With the development of pump cavitation, the amplitudes of pressure fluctuation increase, but when  $NPSHA$  drop to  $1.05\text{m}$ , only appears decreasing on point V8. It is mainly due to the vortex strength weakening.

#### Acknowledgments

This work was supported by the Inner Mongolia Higher School Scientific Research Program [Grant number NJZY17450].

#### References

- [1] Cudina M 2003 *J. of Mechanical Systems and Signal Processing* **17**(6) 1335-1347
- [2] Yao Z F, Wang F J, Xiao R F and He C L 2012 *Pro. of the 26th IAHR Sym. on Hydraulic Machinery and Systems(Beijing, China, August19-23, 2012)*
- [3] Duplaa S, Coutier-Delgosha O, Dazin A, Roussette O, Bois G and Caignaert G 2010 *J. Fluids Eng.* **132** 021301-1
- [4] Leroux J B, Coutier-Delgosha O and Andre Astolfi J 2005 *J. Physics of Fluids* **17** 052101
- [5] Bachert R, Stoffel B and Dular M 2010 *J. Fluids Eng.* **132** 061301-1
- [6] Tan L, Zhu B S, Cao S L, Wang Y C and Wang B B 2014 *P I Mech Eng C-J Mec* **228** 1994-2006
- [7] Tan L, Zhu B S, Cao S L and Wang Y M 2013 *Chinese Sci Bull* **58**(8) 949-52
- [8] Tan L, Cao S L, Wang Y M and Zhu B S 2012 *Chinese Phys Lett* **29**(1) 014702
- [9] Zwart P J, Gerber A G and Belamri T 2004 *Pro.of the 5th ICMF Int. Conf. on Multiphase Flow(Yokohama, Japan, May30-June3, 2004)*
- [10] Meng G Q Q G, Tan L, Cao S L, Wang Y C, Xu Y and Qu W S 2014 *Pro. of the 6th Int. Sym. on Fluid Machinery and Fluids Engineering(Wuhan, China, October22-25, 2014)*
- [11] Liu H L, Wang J, Wang Y, Zhang H and Huang H Q 2014 *Int. J. Nav. Archit. Ocean Eng.* **6** 119-131